Research on All-Fiber Dual-Modulation Optic Current Sensor Based on Real-Time Temperature Compensation

Jianhua Wu, Xiaofeng Zhang, Liang Chen, Benxiang Wu, and Cheng Peng

***Abstract*—We present a method to simultaneously measure the temperature and electric current, which can be applied for the all-fiber optic current sensor (AFOCS) temperature compensation. The Faraday rotation mirror is introduced as the temperature sensing unit based on the all-fiber dual-modulation optic current sensor. The temperature and electric current could be distinguished by the sequence of pulse light received by the photodetector. The working principle of temperature and electric current sensing are analyzed by modeling and simulation. The experiments are designed to confirm the temperature compensation scheme. The relative error of AFOCS decreases from 14% to 2% by temperature compensation, which meets the requirements of micro-current fiber sensing.**

***Index Terms*—Coherent effects, fiber optics systems, sensors.**

I. Introduction

COMPARED with traditional current transducers, the all-fiber optic current sensor (AFOCS) possesses the well-known advantages of small size, insensitivity to electromagnetic interference, wide dynamic range, high frequency bandwidth, safety, electrical isolation, and environmental protection [1]–[3]. To date, AFOCS has been widely applied in the electrolytic aluminum industry [4], ultra high voltage DC power system [5], lightning current measurement [6], and plasma current measurement [7], which are the high-current applications. Meanwhile, AFOCS has attracted significant attention from micro-current detection fields, such as ship leakage current [8], [9] and partial discharge measurement [10].

Unfortunately, the operation characteristics of fiber change with temperature, which will alter the polarization of light in the fiber and affect the measurement accuracy of AFOCS. The influence of temperature on AFOCS is mainly divided into three categories. The first is the Verdet constant of sensing fiber. Xu points out that the Faraday effect (the Verdet constant) varies by 0.7% from -40°C to 60 °C [11]. The second is linear birefringence. The linear birefringence in optical fibers changes with temperature by 0.1%/°C [12]. The last is the phase delay of the quarter-wave plate (QWP). The scale factor of AFOCS varies about 4.5% from −40 °C to 60 °C [13]. Therefore, temperature compensation must be carried out to satisfy the required accuracy for DL/T 1789 class 0.2S [14].

The temperature compensation methods can be classified into four categories, i.e., the heat insulation cavity structure, the adaptive temperature compensation scheme, device temperature stability, and the data processing methods. The heat insulation cavity structure can maintain the sensing head within a constant temperature range [15]. However, the external and internal temperatures will be consistent via the heat exchange. This structure is suitable for areas with temperature that vary dramatically but not ideal for areas with temperature changes slowly. Optical devices realize the adaptive temperature compensation scheme with opposite temperature coefficient symbols. The optical devices are extra [16] or parts of AFOCS [17], [18]. However, the accuracy of optical devices is so high that it is difficult to achieve. Improving the optical device temperature stability [19], [20] or the sensing fiber wrapping method [21] is viable. However, the cost and the accuracy are the major obstacles. Compared with these temperature compensation schemes, the real-time temperature compensation method by data processing [5] is more attractive. This method does not alter the optical devices and serves the purpose of temperature compensation. However, there also are some drawbacks. Firstly, the temperature sensing and electric current sensing units share the same superluminescent diode (SLD) light source and signal processing module [5]. However, the other optical devices are independent, which is harmful for integration. The second is the temperature coefficient being very small (about negative 10^{-3} magnitude [22]). The temperature is obtained by intensity demodulation, which can be submerged in the noise. In this work, we propose and demonstrate a method to measure the temperature and the electric current simultaneously. The electric current and temperature sensing systems share the same light source, transmission fiber line, photodetector (PD), and data processing system, which can improve system integration. The only difference is the sensing units. The temperature

Manuscript received February 2, 2022; revised March 7, 2022; accepted March 21, 2022. Date of publication March 29, 2022; date of current version April 18, 2022. (*Corresponding author: Liang Chen.*)

Jianhua Wu is with the Naval University of Engineering, Wuhan 430033, China, and also with the Institute of No. 92853 Troops, Huludao 125106, China (e-mail: jianhuafly@163.com).

Xiaofeng Zhang, Liang Chen, and Benxiang Wu are with the Institute of College of Electrical Engineering, Naval University of Engineering, Wuhan 430033, China (e-mail: zhangxiaofeng201@126.com; 15038513@alu.hdu.edu.cn; 412647022@qq.com).

Cheng Peng is with the Institute of College of Information and Communication, National University of Defense Technology, Wuhan 430033, China, and also with the Naval University of Engineering, Wuhan 430033, China (e-mail: raul0421@sina.com.cn).

Digital Object Identifier 10.1109/JPHOT.2022.3162114

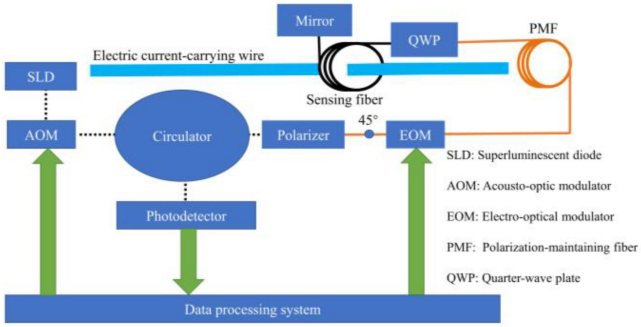

Fig. 1. The schematic diagram of AFOCS with dual-modulation.

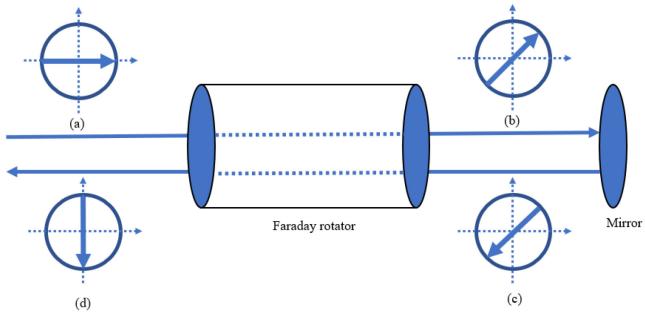

Fig. 2. The polarization evolution by Faraday rotation mirror.

coefficient of the Faraday rotation mirror (FRM) is much more significant. The relative error decreases from 14% to 2% by temperature compensation with the data processing method.

The remainder of this paper is organized as follows. Section II describes the principle of operation. The dual-modulation AFOCS and dual-parameter measurement of temperature and current are introduced in this part; In Section III, we model and simulate to explore the influence of modulation parameters on temperature compensation. The experiments are designed to verify the correctness of the theory in Section IV. The experimental results and discussions are also in this section. The last section is the conclusion.

II. Operating Principle

A. The Principle of Dual-Modulation AFOCS

The acousto-optic modulator (AOM) and electro-optical modulator (EOM) are applied to realize the AFOCS based on the reflected interferometer current sensor, which is called dual-modulation AFOCS [23]. The schematic diagram of AFOCS with dual-modulation is shown in Fig. 1.

The black dotted line, orange line, and solid black line represent the single-mode optical fiber (SMF), the polarization-maintaining fiber (PMF), and the spun highly birefringent fiber, respectively. SMF realizes energy transmission, and PMF can reduce the influence of environmental factors on the polarization state. The spun highly birefringent fiber is applied as the sensing fiber, as shown in Fig. 1. The principle of operation is based on the Faraday effect. AOM is applied to modulate the continuous light of SLD to pulsed light. The initial phase and working frequency of pulsed light are adjustable. The amplitude of pulsed light is the same as continuous light. The pulsed light is linearly polarized after passing through the circulator and the polarizer. The polarized light will convert into two linearly polarized light beams via a 45° splice between the polarizer and PMF. These orthogonal polarization modes convert into left-handed and right-handed circularly polarized waves by QWP. The phase velocities of the two circularly polarized light beams are different, and the difference is proportional to the magnetic field generated by the electric current to be measured. The Faraday rotation angle is applied to represent the rotation angle of the polarization plane. The Faraday rotation angle is doubled when the circularly polarized light beams reflect off the mirror at the end of the sensing fiber and retrace their way through the sensing fiber. The circularly polarized lights are returned to be linearly polarized when they pass through QWP on the return trip. Finally, the two waves are brought back together and interfered at the 45° splice and common input/output polarizer [24]. The light intensity with electric current information is sent to PD through the circulator and processed by the data processing system. EOM is used to modulate the phase and improve the sensitivity of AFOCS. The modulation frequency of EOM is related to the optical path length, which is adjusted by PMF and sensing fiber [25].

The light intensity signal received by PD is given by [23]

$$P_{\text{cout}}(t) = k_c P_{in} \cdot \frac{1+\cos[4\theta - \Delta\varphi_{\text{C}}(t)]}{2} \cdot \frac{1+f(t)}{2} \tag{1}$$

Where P_{in} denotes the optical power of the light source, k_c expresses the proportional coefficient related to the optical path loss, and $\Delta\varphi_C(t) = \varphi(t) - \varphi(t+\tau_C)$ represents the phase difference modulated by EOM. $\varphi(t)$ is the modulated signal in the forward transmitting direction, $\varphi(t+\tau_C)$ expresses the modulated signal in the backward transmitting direction with τ_C time delay. $\theta = NVI$ denotes the Faraday rotation angle, N is the number of turns of the sensing fiber coil wrapped around the electric current-carrying wire. V represents the Verdet constant related to the material of sensing fiber, the working wavelength of the light source, and the operating temperature [26]. I expresses the electric current to be measured. The modulation signal of AOM is the periodic gate signal, which can be described as a square wave signal with DC bias. $f(t)$ represents a periodic square wave signal, which is defined by

$$f(t) = \begin{cases} 1 & nt_d + t \le t_0 + nt_d \\ -1 & t_0 + nt_d \le nt_d + t \le (n+1)t_d \end{cases} \tag{2}$$

Here, $t \ge 0$. t_d and t_0 represent the period and pulse width of the modulation signal, respectively. The duty cycle of the modulation signal is $RD = t_0/t_d$. n denotes a positive integer, which indicates the number of pulse repetition periods.

B. The Principle of Temperature Sensing

FRM is composed of a Faraday rotator and a mirror [27]. The adjustment of the state of polarization (SOP) is shown in Fig. 2.

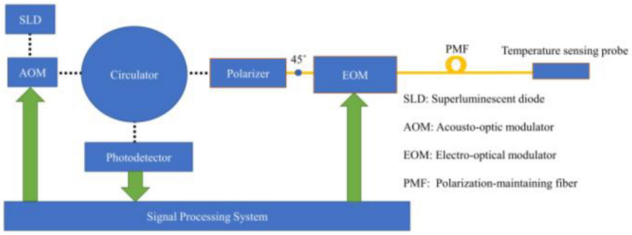

Fig. 3. The schematic of all-fiber optic temperature sensor with dual modulation.

A permanent magnet provides a constant magnetic field for the Faraday rotator. When the propagation direction of the light is consistent with the magnetic induction intensity, the SOP of the light wave will be rotated with an angle of $\pi/4$ rad due to the Faraday effect, as shown in Fig. 2(a) and (b). Then the mirror will reflect the light wave on the far end, and the Faraday rotator will rotate the polarization state with another angle of $\pi/4$ rad in the same direction for the non-reciprocity of Faraday effect, as shown in Fig. 2(c) and (d). Therefore, the polarization direction of the beam will rotate $\pi/2$ rad when FRM is perfect.

The constant magnetic field of FRM is mainly provided by rubidium iron boron materials, which are sensitive to temperature. Therefore, the SOP is affected by temperature. The rotation angle of SOP due to the Faraday rotator is given by

$$\theta_T = \frac{\pi}{4}(1 + a_T \Delta T) \tag{3}$$

Where $\Delta T = T - T_0$ denotes the temperature fluctuation, T_0 is the room temperature (25 °C), and T expresses the operation temperature. a_T represents the temperature coefficient (rad /°C). a_T reflects the relationship between polarization rotation angle and temperature fluctuation.

The schematic of the temperature sensing optical system is shown in Fig. 3.

The temperature sensing probe is FRM in Fig. 3. The continuous light of SLD is modulated to pulsed light by AOM. The frequency is adjustable, and the amplitude is the same as the continuous light. After passing through the circulator, the pulsed light is sent to the polarizer, and then it will change into linearly polarized light. The polarized light will convert into two linearly polarized light beams when the optic axis of the polarizer and EOM is aligned with a 45° offset. The propagation directions are along the fast and slow axes of the polarization-maintaining fiber (PMF), respectively. The state of polarization will change with temperature when FRM reflects them. The polarized beams are brought back together and interfered at the fusion point where the optic axis of EOM and the polarizer is aligned with a 45° offset. EOM is used to modulate the phase and improve the sensitivity. The light intensity received by PD is given by

$$P_{\text{Tout}}(t) = k_T P_{in} \frac{1 + \cos[4\theta_T - \Delta\varphi_{\text{T}}(t)]}{2} \frac{1 + f(t)}{2} \tag{4}$$

Where $P_{\text{Tout}}(t)$ denotes the received light intensity. P_{in} expresses the light power of SLD. k_T represents the proportional coefficient related to the optical path loss. $\Delta\varphi_{\text{T}} = \varphi(t) - \varphi(t + \tau_T)$ denotes the phase difference modulated by EOM. $\varphi(t)$ and $\varphi(t + \tau_T)$ represent the modulated signals in the forward and backward transmitting directions with τ_T time delay. θ_T represents the rotation angle of SOP defined in (3). $f(t)$ denotes a periodic square wave signal defined in (2).

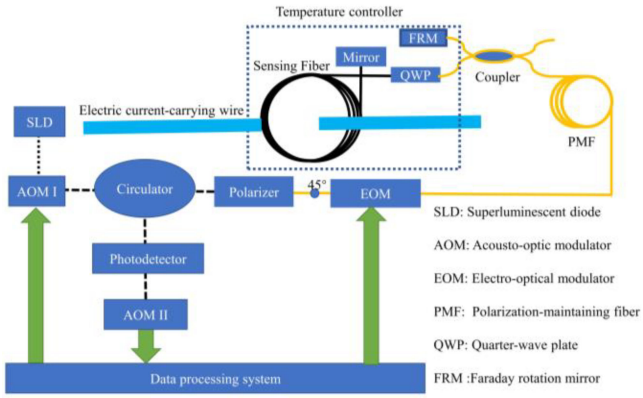

Fig. 4. The schematic diagram of the dual-parameter fiber optical sensor.

C. The Principle of Dual-Parameter Measurement

The optical devices are the same except the fiber sensing units, according to Fig. 3 and Fig. 1. Therefore, the temperature and electric current sensing units are connected with a polarization-maintaining fiber coupler, and the temperature and electric current will be distinguished by the time they return to PD. The schematic diagram of the dual-parameter fiber optical sensor is shown in Fig. 4.

The position of FRM and electric current sensing fiber will be illustrated in part C, Section IV. The simulation parameters are as follows. The coupling ratio of the coupler is 50:50, the proportional coefficients, i.e., k_c and k_T are 0.9 and 0.7, respectively. EOM adopts sine wave modulation. The signal amplitude is 0.921 V, and the modulation frequency is 56.102 kHz. The modulation signals of AOM I and AOM II are the gate signals, and the only difference between them is the initial phase. The amplitude and duty cycle of the modulation signals are 1 V and 25%, respectively. The changes of SOP caused by electric current and temperature are 0.044 rad and 0.001 rad, respectively. The time-domain waveforms received by PD is shown in Fig. 5.

The modulation signals of AOM I and AOM II are the periodic gate signals, which can be seen as switch signals with different initial phases. When the signal of AOM II is "on" all the same, the pulsed light arrives at PD by order because the optical path is different, as shown in Fig. 5(a). The pulsed light with electric current information will reach PD later because the electric current sensing fiber is much longer than the coupler's pigtail. The gate signal of AOM II is used to select the sensing signal by controlling the switch signal's "on/ off". The time when temperature and electric current sensing signals reach PD is different, so we can control the delay time between AOM I and AOM II to get the sensing signal that we select to demodulate, as shown in Fig. 5(b) and (c).

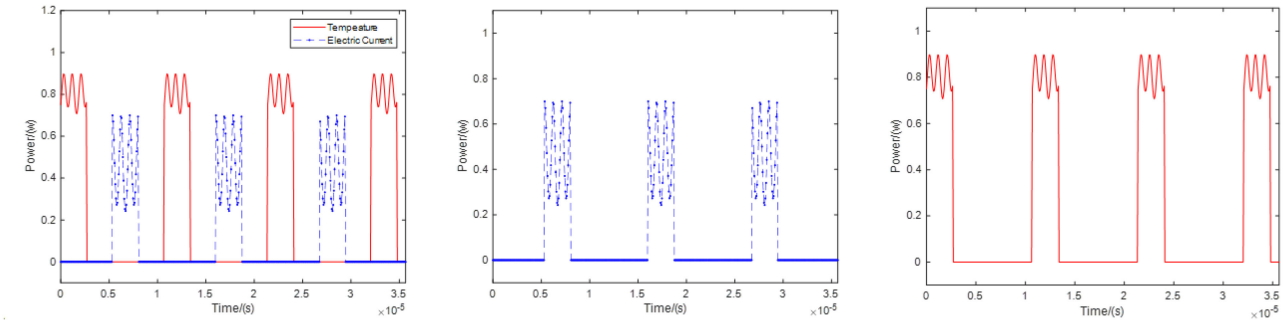

Fig. 5. Time domain-waveform simulation. (a): Time-domain simulation of temperature and current; (b): Time-domain simulation of electric-current; (c): Time-domain simulation of temperature.

III. Modeling and Simulation Analysis

A. Data Demodulation

The temperature and electric current sensing system share the same data processing system. The optical power of the signal received by the photodetector is the sum of the harmonics of the modulation frequency of EOM if the light source is a continuous light source, as described in previous works [28]. The square wave signals can be expanded into the Fourier series, which is the sum of the harmonics of the modulation frequency of AOM. The relevant demodulation method is applied for demodulation to improve the ability of data processing, and the frequency relationship between the AOM and EOM has been described in detail in previous works [23]. The output of relevant demodulation is given by [23]

$$R = -\frac{kRD \cdot P_{in} \cdot J_1(\delta) \cdot \sin\theta}{2} \tag{5}$$

Where R denotes the output of the correlation demodulation, RD represents the duty cycle of AOM, P_{in} expresses the input total light energy. k denotes the proportional coefficient. $k = k_T$ and $k = k_C$ represent the proportional coefficient of temperature and the electric current sensor, respectively. $J_1(\delta)$ expresses the first order Bessel function of the first kind. δ is twice as much as the modulated signal amplitude.

B. The Effect of Temperature on Electric Current Sensing

The Verdet constant, QWP, and the linear birefringence of the sensing fiber are related to temperature. The effect of temperature on electric current sensing can be regarded as a polynomial function, and we use second-order polynomials for the sake of simplicity. The relationship between the Faraday rotation angle and the temperature fluctuation is given by

$$\theta(T) = \theta(T_0) + a\Delta T^2 + b\Delta T + c \tag{6}$$

Where $a\Delta T^2 + b\Delta T + c$ is the additive noise, a, b, and c are the coefficients of quadratic term, primary term, and constant term, respectively. $\Delta T = T - T_0$ represents the temperature fluctuation, T_0 denotes the room temperature (25 °C), T denotes the operation temperature.

C. Relationship Between the Length of PMF and Sensing Fiber

The relationship between the eigenfrequency and fiber total length of dual-parameter fiber optical sensor is given by

$$f_s = c/(2n_0L) \tag{7}$$

Where f_s denotes the eigenfrequency. f_s=f_T and f_s=f_C represent the eigenfrequency of temperature and electric current sensing system, respectively. c expresses the speed of light in vacuum, n_0 and L represent the refractive index and the total fiber length from EOM to the reflection unit, respectively. L=L_{PMF} denotes the length of fiber for the temperature sensing system when the pigtail of the polarization-maintaining fiber coupler is much short than PMF. L=L_{SF}+L_{PMF} represent the sum of PMF and current sensing fiber for an electric current sensing system and L_{SF} denotes the length of the electric current sensing fiber. τ=$1/f_s$ represents the difference between the times taken by the beams to propagate from EOM to the reflection unit for a round trip. For sine modulation, $\varphi(t) = A\sin(2\pi ft)$, where f and A denote the frequency and the amplitude of modulation signal, respectively. The phase difference modulated by EOM is given by

$$\begin{aligned}\Delta\varphi(t) &= \varphi(t) - \varphi(t+\tau) \\ &= -2A\sin\left(\frac{\pi f}{f_s}\right) \cdot \cos\left[2\pi f\left(t + \frac{1}{2f_s}\right)\right]\end{aligned} \tag{8}$$

Equation (5) will convert into

$$R = -\frac{kRD \cdot P_{in} \cdot J_1(\delta') \cdot \sin\theta}{2} \tag{9}$$

Where δ'=$2A\sin(\frac{\pi f}{f_s})$ denotes the modulation factor. We define the ratio of modulation frequency to eigenfrequency as the frequency ratio m, $m = f/f_s$. (9) will be the same as (5) when m equals 1/2.

We define the normalized scale factor χ as

$$\chi = \frac{J_1(\delta')}{max[J_1(\delta')]} \tag{10}$$

We get the maximum for the 1st-order Bessel function of the first kind when δ' equals 1.842 V by calculation. The relationship

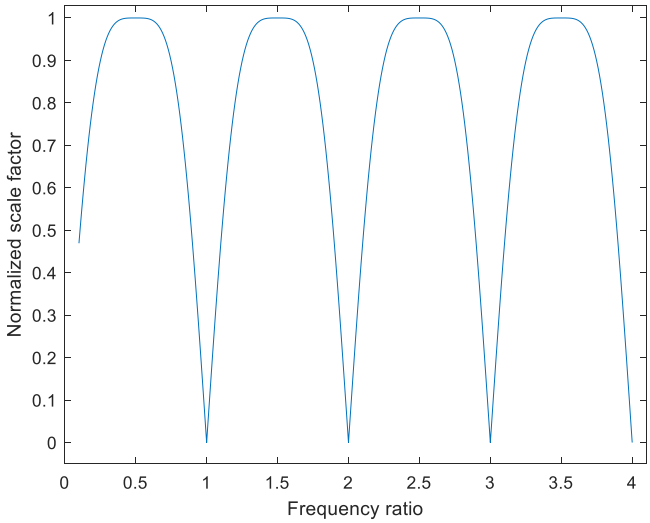

Fig. 6. The relationship between frequency ratio and normalized scale factor.

between the frequency ratio and normalized scale factor is shown in Fig. 6.

The normalized scale factor will get the maximum when the frequency ratio is an odd multiple of 1/2 and the minimum when the frequency ratio is an even multiple of 1/2, as shown in Fig. 6.

The normalized scale factor of temperature and electric current sensing system get the maximum at the same time when the eigenfrequency and the modulation frequency can meet the relationship

$$\begin{cases} f_T = \frac{2f}{2n_1+1} \\ f_C = \frac{2f}{2n_1+2n_2+1} \end{cases} \tag{11}$$

Where f_C and f_T denote the eigenfrequencies of the electric current and the temperature sensing unit, respectively. n_1 and n_2 are both integers, $n_1 \geq 0$, and $n_2 \geq 1$.

According to (7) and (11), the relationship between the length of PMF and electric current sensing fiber can be given by

$$\frac{L_{SF}}{L_{PMF}} = \frac{2n_2}{2n_1+1} \tag{12}$$

Where L_{SF} and L_{PMF} represent the lengths of the electric current sensing fiber and PMF, respectively, as defined in (7).

IV. Experimental Results and Discussions

A. Modulation Frequency Test Experiment and Discussion

1) Experimental Device and Main Parameters: The relationship between the frequency ratio and normalized scale factor is verified before the temperature and electric current measurement experiment because we must determine the fiber length firstly. We used the electric current measurement results to demonstrate the relationship between the frequency ratio and the normalized scale factor. AOM I and AOM II both adopted the continuous optical working mode, which could be regarded as the fixed loss of the optical path. The dual-modulation AFOCS was equivalent to the reflective interference current sensor. The experimental setup is shown in Fig. 7.

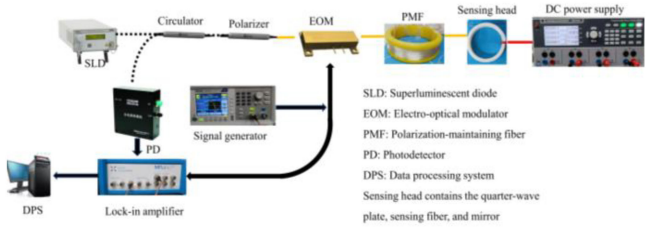

Fig. 7. The experimental setup for frequency test.

TABLE I
The Experimental Equipment and Main Parameters

Equipment or Device	Enterprise or Brand	Model	Main Parameters
Light source	Thorlabs	S5FC1018P	The wavelength is 1310nm, spectral width is 40nm, and the power is 30 mW
EOM	SWT Optics Co. Ltd., Beijing, China	PMS1322-CX-TL	The half-wave voltage is 4 V, insertion loss is 3.5 dB
Photodetector	Conquer Co. LTD., Beijing, China	KG-HSP	Wavelength is from 1100 nm to 1650 nm, and dynamic range is 25 dB
Lock-in amplifier	Zurich Instruments	MFLI 500 kHz	Frequency resolution is 1 μHz, and the phase resolution is 10 μdeg
DC power supply	Rohde & Schwarz, Muenchen, Germany.	R&S®HMP4000	The maximum output current is 10A
Signal generator	Tektronix China Inc., Shanghai, China.	AFG 1062.	The bandwidth is 25 MHz
Circulator	MC Fiber Optics Co. Ltd., Shenzhen, China.	Commercially available	The insertion loss is 0.6 dB
Polarizer	MC Fiber Optics Co. Ltd., Shenzhen, China.	Commercially available	The extinction ratio is no less than 28 dB
Mirror	YOFC Optical Fiber and Cable Co. LTD., Wuhan, China	Commercially available	Reflectivity is greater than 99%@1310 nm
QWP	Do it by ourselves		
PMF	YOFC Optical Fiber and Cable Co. LTD., Wuhan, China	PM1016-A	Beat length is 3 mm
Sensing fiber	YOFC Optical Fiber and Cable Co. LTD., Wuhan, China	SH1016A	Beat length is 10 mm, and the spin pitch is 5 mm

The models and main parameters of optical devices were shown in Table I.

2) Experimental Results and Discussion: The sensing fiber and PFM were 500 m and 200 m, respectively. The eigenfrequency was 151.975 kHz, according to (7). The lock-in amplifier worked at the external modulation mode, and the signal generator provided the modulation signal. The signal generator worked at the sweep mode. The initial frequency was 6 kHz, the termination frequency was 300 kHz, and the frequency step was

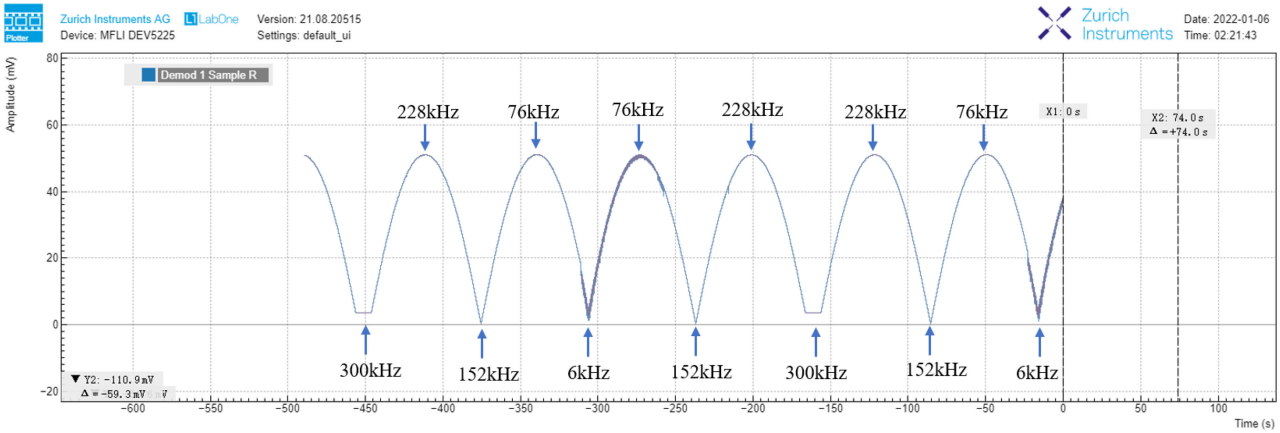

Fig. 8. The screenshot of the lock-in amplifier.

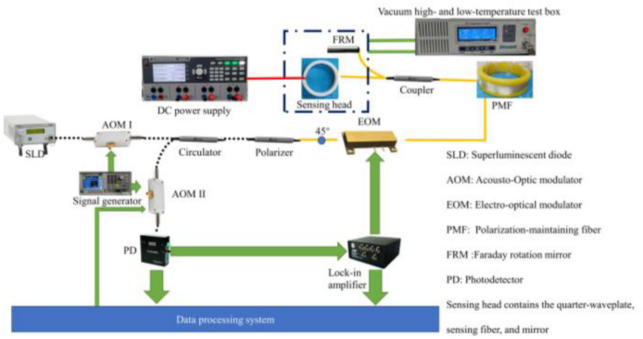

Fig. 9. The experimental setup for the electric current and temperature measurement.

2 kHz. The lock-in amplifier was applied for demodulation. The screenshot of the lock-in amplifier is shown in Fig. 8.

The frequency ratio affected the normalized scale factor, as shown in Fig. 8. The normalized scale factor got the maximum when the frequency ratio was an odd multiple of 1/2 and the minimum when the frequency ratio was an even multiple of 1/2, as analyzed in Part C, Section III. Therefore, the length of PMF and the electric current sensing fiber must be optimal to get the maximum normalized scale factor.

B. Temperature Compensation of Electric Current Sensing

The electric current sensing fiber is the spun highly birefringent fibers, which is fabricated by spinning the fiber perform during the drawing process. The manufacturing process is more complex, and the cost is higher than PMF. Therefore, the length of PMF was adjusted to meet (11). The length of PMF was adjusted to 250 m to satisfy (12) with the polarization-maintaining optical fiber fusion machine.

1) Experimental Device: The experimental setup was adjusted based on Fig. 7, as shown in Fig. 9.

Based on the experimental device in Table I, the models and main parameters of newly introduced optical devices were shown in Table II.

TABLE II
THE EXPERIMENTAL EQUIPMENT AND MAIN PARAMETERS

Equipment or Device	Enterprise or Brand	Model	Main Parameters
AOM	Qingjin(Shanghai) LTd.Co	custom-made	The insertion loss is 2dB, and the extinction ratio is 50dB
Lock-in amplifier	Kongtum (Shanghai) Ltd. Co	QTLIA	frequency⩽500kHz
Vacuum high- and low-temperature test box	Wuhan Tailunte Century Technology Co., Ltd	TLTB-VHLB50	Range: - 60 ℃ - 100 ℃, accuracy ± 0.1 ℃
Coupler	MC Fiber Optics Co. Ltd., Shenzhen, China.	Commercially available	The coupling ratio is 50:50
FRM	MC Fiber Optics Co. Ltd., Shenzhen, China.	Commercially available	Reflectivity is greater than 99%@1310nm

The desktop lock-in amplifier was replaced by modularization for the volume. The coupler was the polarization-maintaining fiber coupler.

2) Experimental Results and Discussion: The temperature of the vacuum high- and low-temperature test box was set from 5 °C to 65 °C, and the temperature step interval was 2 °C. When the temperature reached the setting temperature, kept the temperature for 3 minutes before data acquisition to ensure FRM and the sensing head heated evenly. The data acquisition time was 1 min, and the mean value was used as the measurement result to eliminate the influence of random noise. An external current was provided by the DC power supply, which was constant all over the experimental process.

The relationship between the output of the lock-in amplifier and the temperature is shown in Fig. 10.

The sinusoidal function was applied for data fitting. The fitting function was given by

$$f(T) = a\sin[b(T-25)+c]+d \tag{13}$$

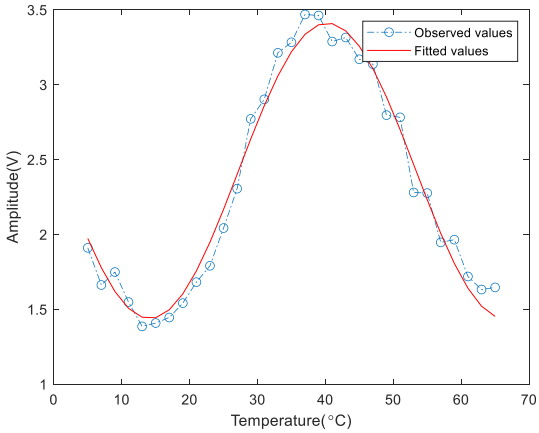

Fig. 10. The relationship between the temperature and the output of temperature sensing.

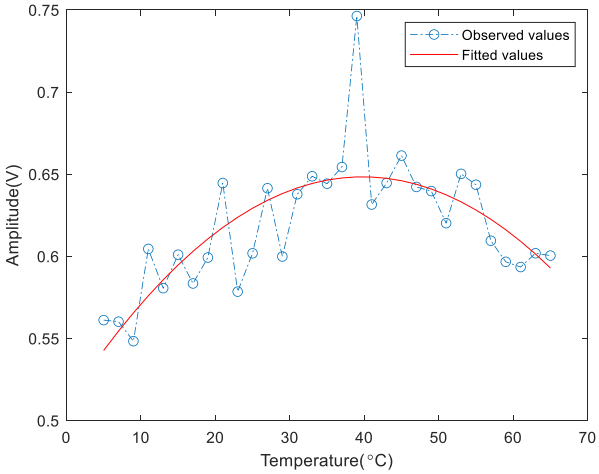

Fig. 11. The relationship between the temperature and the output of electric current sensing (1A).

Where a, b, c, and d were -0.9867, 0.1201, -0.1261, and 2.425, respectively. The correlation coefficient was 0.9782, which indicated that the fitted values were consistent with the observed values. The temperature coefficient of FRM was 0.1201 rad/°C.

The output of the lock-in amplifier was collected at different temperatures with the same electric current (1A). After eliminating the zero bias, the observed values and fitted values are shown in Fig. 11.

The room temperature (25 °C) was set as the reference temperature, and polynomial was used for data fitting. The fitting function was given by

$$y(T) = p_1(T-25)^2 + p_2(T-25) + p_3 \tag{14}$$

Where p_1, p_2, and p_3 were -8.733×10^{-5}, 0.002584 and 0.6293, respectively. The correlation coefficient was 0.5802. The model data did not agree well due to noise interference. However, the fitted values could display the trend of observed values.

The relationship between the temperature and electric current was determined by (13) and (14). When the measured current was 2A, we experimented again under the same experimental

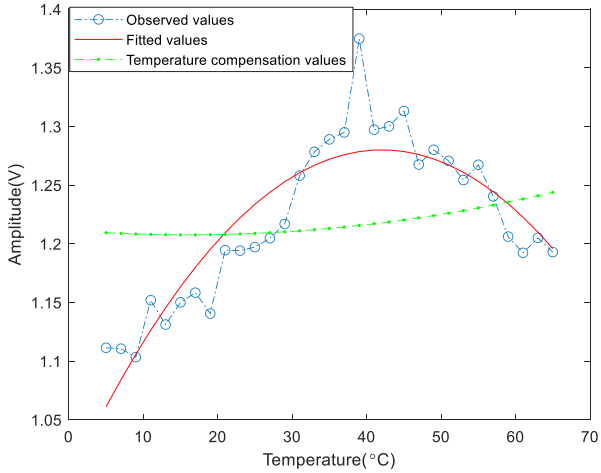

Fig. 12. The relationship between the temperature and the output of electric current sensing (2A).

conditions. The relationship between the output result of the lock-in amplifier and temperature is shown in Fig. 12.

The green dotted line denoted the temperature compensation result using the fitting function described in (14). The dot data represented the observed values when the electric current equaled 2A at different temperatures; The solid red line was the fitted values with a polynomial, and the fitting function was given by

$$y'(T) = p_1'(T-25)^2 + p_2'(T-25) + p_3' \tag{15}$$

Where p', p_2', and p_3' were -0.0001596, 0.005435, and 1.234, respectively. We define the relative error as

$$\eta = \left| \frac{y'(25) + Y(T) - y'(T)}{y'(25)} \right| \tag{16}$$

Where $y'(T)$ denoted the result of the electric current measurement. When the temperature compensation was not carried out, $Y(T) = 0$; If the temperature compensation was performed, $Y(T) = y(T)$.The relationship between the relative error and temperature is shown in Fig. 13.

The relative error fluctuated greatly with the temperature when the temperature compensation was not carried out, as shown in Fig. 13 with a blue circle dotted line. The maximum value declined from 14% to 2% by temperature compensation, as shown in Fig. 13 with a red-point dotted line.

C. Discussion About the Temperature Sensing Unit

1) Installation Position of FRM: The precondition of the Faraday effect is that a light beam traveling in a transparent medium and an external magnetic field is aligned with the light wave propagation vector. Therefore, we should install the FRM in the position where the external magnetic field generated by the electric current is perpendicular to the beam reflected by the FRM. The electric current will have no business on temperature sensing. The installation is shown in Fig. 14

The reflection mirror and the QWP are adjacent to meet the Ampere circuit theorem. FRM is close to QWP to sensing the

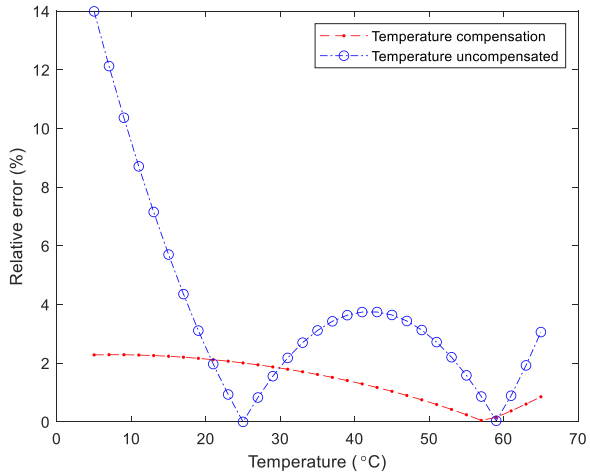

Fig. 13. The relationship between the relative error and temperature.

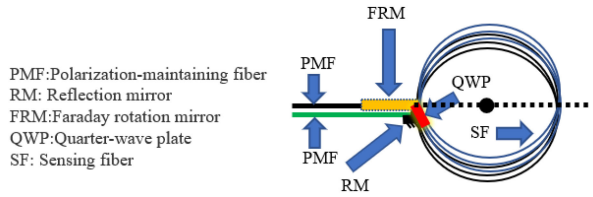

Fig. 14. Installation position of temperature and the electric current sensing unit.

temperature fluctuation. The extension line of PMF and FRM passes through the center of the electric current sensing ring, as shown in Fig. 14

2) Influence of Electric Current on FRM: The electric current is enormous, especially when the electric current is the impulse current, the magnetic induction intensity generated by the electric current will affect FRM. When the magnetic induction intensity generated by the electric current is far less than the change of permanent magnet magnetic induction intensity by temperature (less than 1%), the influence magnetic field generated by the electric current can be ignored. The temperature coefficient of FRM is 0.1201 rad/°C. The maximum electric current to be measured is 1092.82 A by calculation.

3) The Operating Range of FRM: The magnetic induction intensity of permanent magnet materials is affected by temperature, and there is a demagnetization phenomenon when the temperature reaches Curie temperature. The Curie temperature usually is higher than 300°C [29], which is higher than the normal temperature range of AFOCS. Therefore, the temperature sensing by FRM can be applied for AFOCS temperature compensation all over the operating temperature range. However, the optimal operating temperature range is 14 °C - 40 °C when the output of the lock-in amplifier is linear with the temperature, as shown in Fig. 10. If the temperature exceeds this range, the temperature sensing system needs to be calibrated before operation.

4) Optical Path Loss: The energy of the optical path is attenuated by 3dB based on the original power when we introduce the coupler (coupling ratio 50:50), which will have an adverse impact on the signal-to-noise ratio [30]. The influence of the coupler on the signal-to-noise ratio can be compensated by increasing the input optical power.

V. Conclusion

We have demonstrated a dual-modulation all-fiber optic current sensor with temperature compensation by FRM. Both theoretical analysis and experimental results indicate that the proposed method is effective. The temperature and electric current sensing units share the same optical devices except for the sensing units, which can meet integration requirements. The relative error of AFOCS declines from 14% to 2% when the temperature compensation is applied. This sensor can be used to ship leakage current, partial discharge measurement, and other micro-current measurement fields.

Acknowledgment

The authors would like to thank anyone for his constructive advice.

References

[1] P. Mihailovic and S. Petricevic, "Fiber optic sensors based on the Faraday effect," *Sensors*, vol. 21, no. 19, 2021, Art. no. 6564.
[2] K. Bohnert, P. Gabus, J. Nehring, and H. Brandle, "Temperature and vibration insensitive fiber-optic current sensor," *J. Lightw. Technol.*, vol. 20, no. 2, pp. 267–276, Feb. 2002.
[3] R. Wang, S. Xu, W. Li, and X. Wang, "Optical fiber current sensor research: Review and outlook," *Opt. Quantum Electron.*, vol. 48, no. 9, 2016, Art. no. 442.
[4] X. Wang, F. Ma, J. Yu, X. Liu, and N. Song, "Design of the portable fiber-optic current transformer for electrolytic aluminum industry," *Optik*, vol. 205, 2020, Art. no. 164187.
[5] J. Zhao, L. Shi, and X. H. Sun, "Design and performance study of a temperature compensated ±1100 kV UHV DC all fiber current transformer," *IEEE Trans. Instrum. Meas.*, vol. 70, 2021, Art. no. 7001206.
[6] J. M. Ge, Y. Shen, W. B. Yu, R. T. Liu, W. Fan, and Y. X. Yang, "A lightning current measurement method based on optical sensing technology," *IEEE Sens. J.*, vol. 19, no. 11, pp. 4250–4258, Jun. 2019.
[7] A. Gusarov *et al.*, "Performance assessment of plasma current measurement at JET using fibre optics current sensor," *Fusion Eng. Des.*, vol. 165, no. 8, 2021, Art. no. 112228.
[8] J. Wu, X. Zhang, L. Chen, and B. Wu, "Research on measurement technology of ship leakage current by all-fiber optic current sensor," *IEEE Access*, vol. 9, pp. 160268–160276, 2021.
[9] J. Wu, X. Zhang, L. Chen, C. Pneg, and B. Wu, "Research progress of All-fiber optic micro-current sensor," (in Chinese), *Laser Optoelectron. Prog.*, vol. 59, no. 17, 2022, Art. no. 1700004.
[10] G. F. Xin *et al.*, "Polarization error analysis of an all-optical fibre small current sensor for partial discharge," *J. Electr. Eng. Technol.*, vol. 15, no. 5, pp. 2199–2210, 2020.
[11] Y. Xu, D. P. Lu, Q. S. Bu, and Y. B. Yuan, "Analysis for effect of Fiber-optic current transformer on protection accuracy and reliability," (in Chinese), *Automat. Electric Power Syst.*, vol. 37, no. 16, pp. 119–124, 2013.
[12] S. X. Short, A. A. Tselikov, J. U. de Arruda, and J. N. Blake, "Imperfect quarter-waveplate compensation in sagnac interferometer-type current sensors," *J. Lightw. Technol.*, vol. 16, no. 7, pp. 1212–1219, Jul. 1998.
[13] X. X. Wang, C. X. Zhang, C. Y. Zhang, and Z. J. Wu, "Research on temperature characteristic of Quarter-waveplate and its effect on fiber optical current transformers," (in Chinese), *Laser Nfrared*, vol. 7, pp. 596–598, 2006.
[14] *Chinese Electric Power Industry Criteria for Technical Specification for Fiber Optic Current Transformers*, Chinese Industry Standaed DL/T 1789, China, 2017.

[15] H. Yang, L. Qiao, Y. Yang, W. Huang, and S. Sun, "Thermally induced error analysis and suppression of optic fiber delay loop in the different variable rate of temperature," *Optik*, vol. 193, 2019, Art. no. 162994.
[16] K. Sasaki, M. Takahashi, and Y. Hirata, "Temperature-insensitive Sagnac-type optical current transformer," *J. Lightw. Technol.*, vol. 33, no. 12, pp. 2463–2467, Jun. 2015.
[17] G. M. Muller, X. Gu, L. Yang, A. Frank, and K. Bohnert, "Inherent temperature compensation of fiber-optic current sensors employing spun highly birefringent fiber," *Opt. Exp.*, vol. 24, pp. 11164–11173, 2016.
[18] G. M. Muller, A. Frank, L. Yang, X. Gu, and K. Bohnert, "Temperature compensation of interferometric and polarimetric fiber-optic current sensors with spun highly birefringent fiber," *J. Lightw. Technol*, vol. 37, no. 18, pp. 4507–4513, Sep. 2019.
[19] N. Peng *et al.*, "Fiber optic current sensor based on special spun highly birefringent fiber," *IEEE Photon. Technol. Lett.*, vol. 25, no. 17, pp. 1668–1671, Sep. 2013.
[20] R. Zhang *et al.*, "Polarization-maintaining photonic crystal fiber based quarter waveplate for temperature stability improvement of fiber optic current sensor," *J. Mod. Opt.*, vol. 60, pp. 963–969, 2013.
[21] W. Wang, X. F. Wang, and J. L. Xia, "The nonreciprocal errors in fiber optic current sensors," *Opt. Laser Technol.*, vol. 43, pp. 1470–1474, 2011.
[22] Y. H. Yang, "Temperature sensor based on PNR in Sagnac interferometer," *Chin. Opt. Lett.*, vol. 2, no. 5, pp. 259–261, 2004.
[23] J. Wu, X. Zhang, and L. Chen, "Research on the dual modulation of all-fiber optic current sensor," *Sensors*, vol. 22, 2022, Art. no. 430.
[24] J. Blake, P. Tantaswadi, and R. Carvalho, "In-line Sagnac interferometer current sensor," *IEEE Trans. Power Del.*, vol. 11, no. 1, pp. 116–121, Jan. 1996.
[25] F. B. Pang, Y. Liu, Y. B. Yuan, and L. Gao, "Influencing factors analysis on the detector output signal of fiber optic current transformer with sine modulation," *Measurement*, vol. 151, 2020, Art. no. 107151.
[26] W. Cai, J. H. Xing, and Z. Y. Yang, "Contributions to verdet constant of magneto-optical materials," *Acta Phys. Sin.*, vol. 66, no. 18, pp. 1–7, 2017.
[27] P. Drexler and P. Fiala, "Utilization of Faraday mirror in fiber optic current sensors," *Radioengineering*, vol. 17, pp. 101–107, 2008.
[28] V. Temkina, A. Medvedev, and A. Mayzel, "Research on the methods and algorithms improving the measurements precision and market competitive advantages of fiber optic current sensors," *Sensors*, vol. 20, no. 21, 2020, Art. no. 5995.
[29] Find materials, "Curie temperature and working temperature of sintered Nd-Fe-B," CSDN, Jul. 2020. Accessed: Apr. 9, 2022. [Online]. Available: https://blog.csdn.net/sn20020852/article/details/107060174
[30] B. Hu *et al.*, "Noise analysis and SNR optimization design of fiber optical current transformers," (in Chinese), *High Voltage Eng.*, vol. 43 no. 2, pp. 654–660, 2017.